



Solar Orbiter Observations of Proton and Alpha Particle Kinetic Signatures Related to the Presence of Switchbacks in the Inner Heliosphere: A Case Study

Denise Perrone¹ , Adriana Settino² , Silvia Perri³ , Raffaella D'Amicis⁴ , Rossana De Marco⁴ , Georgios Nicolaou⁵ ,
Daniele Telloni⁶ , Roberto Bruno⁴ , and Christopher J. Owen⁵

¹ ASI—Italian Space Agency, via del Politecnico snc, I-00133 Rome, Italy; denise.perrone@asi.it

² Space Research Institute, Austrian Academy of Sciences, Graz, Austria

³ Dipartimento di Fisica, Università della Calabria, Rende, Italy

⁴ National Institute for Astrophysics, Institute for Space Astrophysics and Planetology, Via del Fosso del Cavaliere 100, I-00133 Rome, Italy

⁵ Department of Space and Climate Physics, Mullard Space Science Laboratory, University College London, Dorking, Surrey, RH5 6NT, UK

⁶ National Institute for Astrophysics, Astrophysical Observatory of Torino, Via Osservatorio 20, I-10025 Pino Torinese, Italy

Received 2024 March 21; revised 2024 July 19; accepted 2024 July 19; published 2024 September 30

Abstract

We investigate how ions, namely protons and alpha particles, kinetically react to the presence of strong deflections in the magnetic field, the so-called switchbacks, in the first stream of slow Alfvénic wind observed by Solar Orbiter at the heliocentric distance of 0.64 au. We focus on an isolated, large-scale switchback, and we study in detail ion kinetic properties. Beyond the expected correlation between the magnetic deflection and ion velocity related to the Alfvénic nature of the switchbacks, we find that, within the switchback, proton and alpha particle densities increase, suggesting ongoing wave activity. Very interestingly, we observe a clear correlation between the magnetic deflection and alpha particle temperature, while no correlation has been found with proton temperature. This is an indication of a possible role played by switchbacks in preferentially heating heavy ions. Our results suggest that the presence of switchbacks can induce a deformation of the proton velocity distribution function, while the preferential heating of alpha particles could be due to a denser secondary beam and a smaller relative drift speed between the beam and core.

Unified Astronomy Thesaurus concepts: [Solar wind \(1534\)](#); [Heliosphere \(711\)](#); [Interplanetary turbulence \(830\)](#)

1. Introduction

Magnetic switchbacks are large deflections of the magnetic field, lasting from seconds to hours, which occur simultaneously with a sudden increase in the radial solar wind velocity. Although they have been previously observed in fast streams of both the polar solar wind by the Ulysses spacecraft (Balogh et al. 1999; Yamauchi et al. 2004) and the inner heliosphere, within Mercury's orbit, by the Helios satellites (Borovsky 2016; Horbury et al. 2018), only recently have the nature and origin of switchbacks gained interest for interpreting the solar wind dynamics (see, e.g., Raouafi et al. 2023). Indeed, since the first observations of Parker Solar Probe (Fox et al. 2016), switchbacks have frequently been observed in patches, separated by periods of an almost steady and radial magnetic field, in the near-Sun environment (Bale et al. 2019; Kasper et al. 2019; Horbury et al. 2020a; Dudok de Wit et al. 2020; Larosa et al. 2021; Pecora et al. 2022). Switchbacks are almost Alfvénic in nature, since they are characterized by a high degree of correlation between magnetic and velocity fluctuations, keeping a nearly constant magnetic field intensity, and they appear as S-shaped magnetic structures (McManus et al. 2020). These structures are not aligned along the background direction of the flow but instead aligned along the local Parker spiral, suggesting that they could propagate along the magnetic field (Laker et al. 2021). Although the proton core temperature seems to not change inside each individual switchback (Woolley et al. 2020; Martinović et al. 2021), the observed

patches seem to be hotter with respect to the background plasma (Bale et al. 2019; Woodham et al. 2021; Laker et al. 2024). In particular, Woodham et al. (2021) showed that the parallel temperature is enhanced inside patches of switchbacks, which last for tens of minutes and do not rotate more than 90°, while the perpendicular one remains mostly constant, even though it is higher than the parallel one. Extending the results of Woodham et al. (2021), Laker et al. (2024) found that both the parallel and perpendicular proton temperatures increase inside switchbacks, an aspect that is related to the magnetic field angle. This suggests that the observed temperature enhancement can be generated by some local mechanisms in the near-Sun environment. Finally, Huang et al. (2023a) statistically compared the proton and alpha temperature differences inside and outside switchbacks, considering fully reversed structures, but the deflection is only in the radial magnetic component. In particular, they found that inside patches of switchbacks, the proton temperature is mainly driven by parallel heating with a relatively smaller amount of perpendicular heating. On the other hand, the ratio between alpha and proton temperatures is larger outside the spike, suggesting opposite features for alpha particles with respect to protons.

Despite the growing interest in this area of research, the mechanisms responsible for the generation of switchbacks are still an open question (Huang et al. 2023b; Raouafi et al. 2023). Indeed, several works suggest that the origin of switchbacks could be found either locally in the interplanetary space (Squire et al. 2020; Larosa et al. 2021; Macneil et al. 2021; Mallet et al. 2021; Schwadron & McComas 2021; Agapitov et al. 2022) or from the Sun (Nistico et al. 2010; Horbury et al. 2020a; Fargette et al. 2020, 2022; Fisk & Kasper 2020; Zank et al. 2020;



Original content from this work may be used under the terms of the [Creative Commons Attribution 4.0 licence](#). Any further distribution of this work must maintain attribution to the author(s) and the title of the work, journal citation and DOI.

Drake et al. 2021; Kasper et al. 2021; de Pablos et al. 2022; Telloni et al. 2022; Wyper et al. 2022).

Recently, Larosa et al. (2021) studied the statistical properties of switchbacks, with a special focus on their boundaries, in the slow Alfvénic solar wind observed by Parker Solar Probe during its first encounter. They found, by using the ratio between the average magnetic field magnitude inside and the average magnetic field magnitude outside selected switchbacks, two different type of structures, namely, Alfvénic (if the ratio is between 0.95 and 1.05) and compressible (if the ratio is less than 0.95 or larger than 1.05). The occurrence of the Alfvénic structures is more frequent with respect to the compressible ones. Moreover, Larosa et al. (2021) found that most of the observed switchbacks show a significant density variation from outside to inside, even when the magnetic field strength remains almost constant. Finally, they observed the presence of both tangential and rotational discontinuities at the boundaries of these structures, as also reported by different authors (Krasnoselskikh et al. 2020; Akhavan-Tafti et al. 2021; Farrell et al. 2021; Froment et al. 2021; Bizien et al. 2023). In particular, Krasnoselskikh et al. (2020) found that the strong discontinuities at the switchback boundaries are associated with an enhancement of the radial Poynting flux, suggesting that some boundary regions may be unstable with respect to the Kelvin–Helmholtz instability (Kasper et al. 2019; Mozer et al. 2020; Larosa et al. 2021).

Although most of the studies on switchbacks are based on Parker Solar Probe measurements, Solar Orbiter (Müller et al. 2020) is giving its contribution in studying the kinetic properties of the proton population and the variability of their velocity distribution functions (VDFs). Louarn et al. (2021) described the modification of proton VDFs linked to the presence of a switchback. In particular, a magnetic spectral analysis showed that this structure corresponds to a quieter state of plasma than its environment. Moreover, the internal part of this switchback is characterized by a complete relaxation of the total temperature anisotropy. The transition from the external anisotropic to the internal isotropic plasma is mostly associated with a decrease of the proton beam relative density. On the other hand, Fedorov et al. (2021) found a different behavior for the proton VDFs related to a switchback-like structure observed by Solar Orbiter at about 1 au. Indeed, they found that inside the switchback, the VDF shows a perpendicular temperature anisotropy, while at the boundaries, the anisotropy is in the parallel direction, typically observed in the reconnection exhaust.

In this paper, we focus on the rarefaction region of the slow Alfvénic wind observed by Solar Orbiter in 2020 July (D’Amicis et al. 2021). This interval represents the first observation of the slow Alfvénic solar wind measured by Solar Orbiter during its cruise phase at the heliocentric distance of 0.64 au. The origin of this stream has been identified in a coronal pseudostreamer configuration. This topology allows the formation and development of twin filament channels related to an anomalous expansion rate (Panasenco et al. 2019). Recently, the nature of turbulent magnetic fluctuations around proton scales has also been studied in the same interval (Perrone et al. 2023). Moreover, coherent structures and related kinetic effects of both proton and alpha particle VDFs have been investigated. Indeed, Perrone et al. (2023) found a strong correlation between the presence of coherent structures,

namely, current sheets and vortices (which also appear in chains), and strong deformations of the ion VDFs.

Here, we study the presence of switchbacks in the rarefaction region of the abovementioned slow Alfvénic interval, and, in particular, we focus on an isolated, large-scale magnetic deflection, with special attention to the kinetic properties of the ions, namely, protons and alpha particles. The paper is organized as follows. In Section 2, we present Solar Orbiter observations within the rarefaction region of the slow Alfvénic interval at 0.64 au, along with the identification of switchbacks; in Section 3, we focus on a very isolated large-scale switchback and the related kinetic properties of the ions; and in Section 4, we summarize the results and discuss our conclusions.

2. Interval Characterization

We consider a portion of the rarefaction region of the slow Alfvénic interval observed by Solar Orbiter in 2020 July at a radial distance of about 0.64 au (D’Amicis et al. 2021; Perrone et al. 2023). In particular, we focus on the full-cadence measurements available for the magnetic field vector (64 Hz) from the fluxgate magnetometer (Horbury et al. 2020b), electron data with a resolution of 10 s from the Electron Analyser System (Nicolaou et al. 2021), and reprocessed ion data sampled at 4 s resolution from the Proton and Alpha particle sensor (PAS) of the Solar Wind Analyser (SWA) suite (Owen et al. 2020). For the ion data, an innovative method based on the statistical technique of clustering has been directly applied to the full 3D VDFs measured by PAS to separate the core and beam for both protons and alpha particles and derive their moments (De Marco et al. 2023; Bruno et al. 2024). The entire process, from the data cleaning to the validation of the results, is described in De Marco et al. (2023), where up to three ion populations can be identified. Moreover, the algorithm has been upgraded to separate up to four ion populations (Bruno et al. 2024). The number of groups to identify is an input parameter in the process. The moments are then computed for each separated velocity distribution. In the present study, we use moments of the total VDF (core plus beam) for both protons and alpha particles; that is, the input parameter for the group number is two. In the last part of the analysis, in order to interpret the observed kinetic features on ions, we use four groups, thus separating the core and beam for both protons and alpha particles.

2.1. Data Selection

In Figure 1, we consider the first part of the rarefaction region, identified in D’Amicis et al. (2021), between 19:12 UT on July 16 and 10:48 UT on July 17. Panels (a) and (b) show the radial component (blue) and magnitude (black) and the tangential (red) and normal (green) components of the magnetic field vector, respectively. Several deflections of the radial component, B_r , are recovered, despite the almost constant magnitude observed. Indeed, B_r strongly fluctuates and sometimes becomes zero or even negative. Panel (c) displays the proton (green) and alpha particle (violet) speeds. Here we consider the moments of the total VDF (core plus beam) for both protons and alpha particles. We can observe local enhancements in ion speeds that, jointly with local changes in the $\cos \theta_{BV}$ (black line in panel (d)), namely, the cosine of the angle between the proton velocity and the magnetic field vector, are associated with the strongest magnetic field

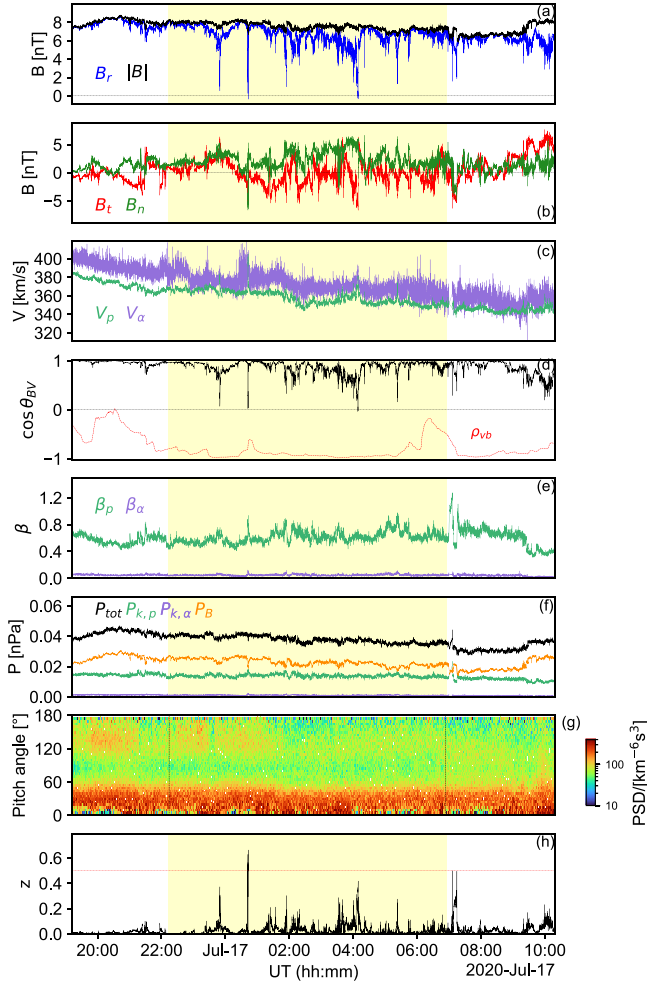


Figure 1. Overview of solar wind data in the rarefaction region of the slow Alfvénic wind observed by Solar Orbiter in 2020 July at 0.64 au (D’Amicis et al. 2021; Perrone et al. 2023). From top to bottom: radial component (blue) and magnitude (black) of the magnetic field vector (a); tangential (red) and normal (green) components of the magnetic field vector (b); proton (green) and alpha particle (violet) speed (c); cosine of the angle between the proton velocity and magnetic field vectors (black) and the v - b correlation coefficient, ρ_{vb} , computed on a 30 minute scale (red) (d); proton (green) and alpha particle (violet) plasma beta (e); kinetic pressure for protons ($P_{k,p}$ in green) and alpha particles ($P_{k,\alpha}$ in violet), magnetic pressure, P_B , in red and total pressure, P_{tot} , in black (f); strahl electron PAD averaged over energies larger than ~ 70 eV (g); and the dimensionless normalized deflection, z , defined in Equation (1) (h). The horizontal red dashed line indicates $z = 0.5$, which corresponds to a magnetic field deflection of 90° with respect to the local average. The yellow shaded band and dashed vertical lines in panel (g) denote the interval considered for the present analysis.

reversals. This correlation is less clear for alpha particles being the signal more affected by noise because of lower counts for their VDF. In panel (d), we also observe that, in the whole considered interval, the average value of $\cos \theta_{BV}$, which is around 1, suggests that Solar Orbiter is sampling a parallel turbulence. In panel (d), the red dashed line represents the v - b correlation coefficient, ρ_{vb} , computed at 30 minute scales. Although we are looking at the rarefaction region of a slow Alfvénic wind, the Alfvénic correlation is still very high, except at the beginning of the considered interval and at the end of the yellow shaded band, where ρ_{vb} reaches values around 0. To better characterize this interval, in panel (e), we show the ion plasma beta, β , defined as the ratio between proton (green) and alpha particle (violet) kinetic, $P_{k,p}$ and $P_{k,\alpha}$, and magnetic,

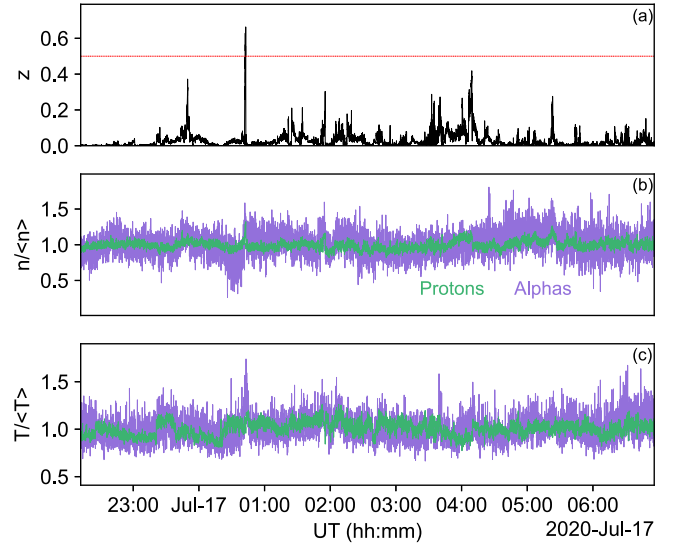


Figure 2. Panel (a): dimensionless normalized deflection, z , as in panel (h) of Figure 1. Panels (b) and (c): normalized density and temperature, respectively, for both protons (green) and alpha particles (violet).

P_B , pressures, which are also separately shown in panel (f) together with the total pressure (in black), $P_{tot} = P_{k,p} + P_{k,\alpha} + P_B$. Panel (g) displays the strahl electron pitch angle distribution (PAD) with energies $E > 70$ eV, where electrons mostly streaming along the mean magnetic field and antiparallel to it can be recognized. Since the magnetic field is almost radial within the selected interval, the strahl radially flows both outward and inward.

Finally, in panel (h), we present the normalized deflection measure, z , as defined by Dudok de Wit et al. (2020),

$$z = \frac{1}{2} [1 - \cos \alpha], \quad (1)$$

where α is the angle between the pointwise magnetic field, \mathbf{B} , and a local average magnetic field, $\langle \mathbf{B} \rangle$, evaluated on a running window of 6 hr. It is worth noting that the definition of z (Dudok de Wit et al. 2020) uses the total magnetic field vector and not only the radial component, even if most of the time B_r is the component showing the largest deflections. The horizontal red dashed line indicates $z = 0.5$, which corresponds to a magnetic field deflection of 90° with respect to $\langle \mathbf{B} \rangle$. A very strong deflection is recovered between 00:41 UT and 00:43 UT on July 17, with $z > 0.5$ and associated with a significant enhancement of the proton speed. The detailed analysis of this structure will be discussed later in the paper. Then, a double peak with $z \simeq 0.5$ is found at 07:12 UT, but it is related to a different behavior in the plasma parameters (see, e.g., ion pressures) and magnetic field magnitude. Therefore, we decide to reduce the interval between 22:12 UT on July 16 and 06:56 UT on July 17 (yellow shaded band and dashed vertical lines in panel (g)), and, in the following, we will refer to this reduced interval.

Figure 2 shows how ion density and temperature react to the presence of deflections in the magnetic field, thus giving information about switchbacks. We remember that the ion moments have been evaluated taking into account the total VDF (core plus beam) for both protons and alpha particles. We observe enhancements in both normalized density (panel (b))

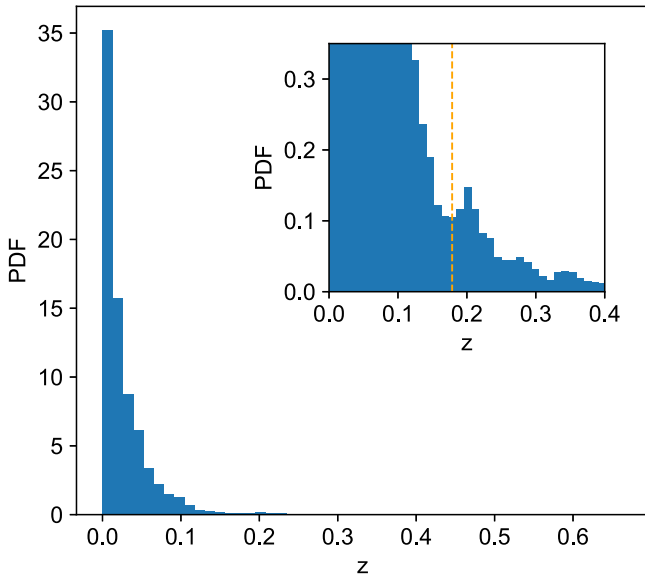


Figure 3. Probability distribution function of z . The insert shows a zoom of the PDF to highlight the presence of a secondary, even smaller, bump. The vertical orange dashed line, $z \approx 0.18$, separates the two populations, and it is used in this study as the threshold to select switchbacks.

and temperature (panel (c)) for both protons (green) and alpha particles (violet) associated with magnetic field reversals (panel (a)). Here, density and temperature are normalized to their averaged values evaluated, as for z , on a running window of 6 hr. Larger fluctuations are recovered in the alpha particle signal with respect to protons due to their lower counts. It is worth noting that a link between magnetic deflections and increases in density and temperature also appears for $z < 0.5$, suggesting that, for statistical studies, it is crucial to identify a suitable threshold for switchback selection. Indeed, the probability distribution function (PDF) for the parameter z , shown in Figure 3, displays a very sharp distribution for very low values of z . However, a zoom of z , in the inset of Figure 3, highlights the presence of a secondary bump. The separation between the two populations is at $z = z^* \approx 0.18$, indicated in the plot by a vertical orange dashed line. This threshold value, z^* , corresponds to magnetic field deflections of 50° with respect to the locally averaged field. $z \geq z^*$ will be the criterion employed in this study to define and select switchbacks.

3. Isolated Large-scale Switchback

Here, we focus on a case study, picking up the strongest deflection found in our interval, in order to give insight into the kinetic effects around and within such structures. Looking in detail at the typical signatures of a switchback, in Figure 4, we present a very isolated, large-scale structure. Panel (a) shows the dimensionless normalized deflection, z , that is well above the selected threshold, z^* (red horizontal dashed line). The vertical dashed lines delimit the structure ($z \geq z^*$). For this particular switchback observed by Solar Orbiter on July 17, z reaches values larger than 0.5; namely, the magnetic deflection is larger than 90° . Indeed, for this isolated switchback, z reaches a value of 0.67, corresponding to a magnetic deflection of about 150° . Panel (b) shows the time series of the magnetic field, where the magnitude is in black and the components, in the RTN reference frame, are radial in blue, tangential in red, and normal in green. As expected, the variation of the magnetic

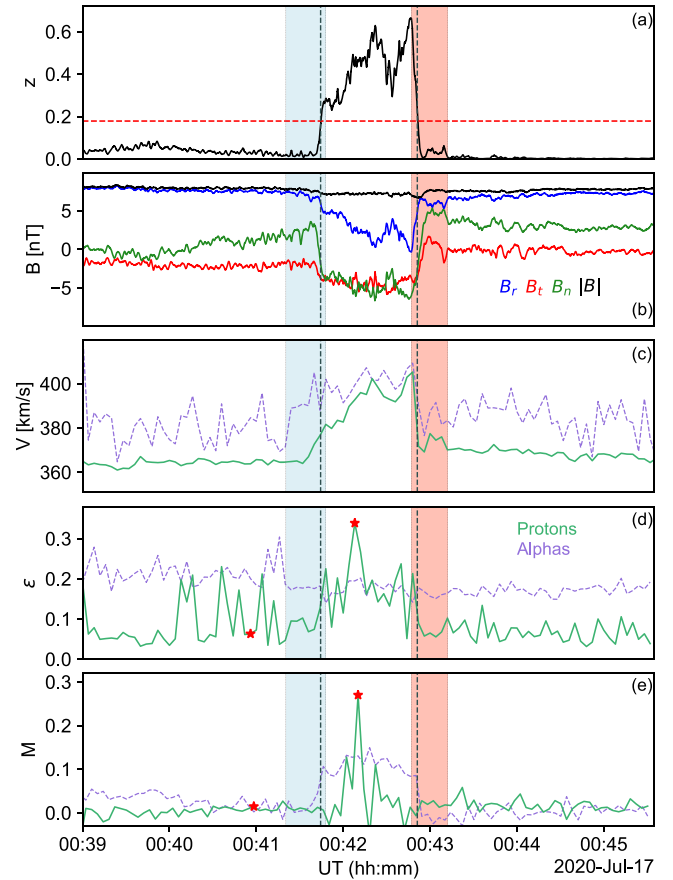


Figure 4. Panel (a): dimensionless normalized deflection, z , with the threshold, $z^* \approx 0.18$, indicated by a red horizontal dashed line. Panel (b): components in RTN (radial in blue, tangential in red, and normal in green) and magnitude (in black) of the magnetic field vector. Panel (c): proton (green) and alpha particle (violet) speed. Panels (d) and (e): two non-Maxwellian parameters, ϵ and M , respectively, for protons (green) and alpha particles (violet). The blue shaded band denotes the leading region, while the red shaded band denotes the trailing region. Vertical dashed lines delimit the structure ($z \geq z^*$). Red stars mark the two times, one outside and the other inside the switchback, at which both the proton and alpha particle VDFs are plotted in Figures 6 and 7, respectively.

field is observed in the total magnetic field vector and not only in one component. Indeed, this is the effect of the rotational nature of switchbacks.

The variation of the magnetic field components is associated with a corresponding variation in the velocity field components (not shown) due to the Alfvénic nature of the switchback. Panel (c) of Figure 4 displays the proton (green) and alpha particle (violet) speeds, evaluated as the moment of the total (core plus beam) VDF for both protons and alpha particles. The proton speed follows the profile of z , with a relative increase of more than 10%, while the enhancement of the alpha speed, of about 10%, starts before the increase of the proton speed, in the region highlighted by a blue shaded band, where the magnetic field components start deflecting. This region is identified as the leading region of the structure. The red shaded band denotes the trailing region, after the switchback, where we observe changes in the magnetic field with respect to the background magnetic field but also in the proton speed, namely, a bump. The latter is also observed in the alpha particle speed, but their signal shows more fluctuating behavior over the entire period. The limits of the characteristic intervals of this structure are summarized in Table 1. It is worth noting that we consider as background the averaged values of the

Table 1

Limits of the Characteristic Intervals of the Switchback Shown in Figure 4 and Observed by Solar Orbiter on July 17

| Regions | Start (UT) | End (UT) |
|-----------------------|------------|------------|
| Switchback | 00:41:44.4 | 00:42:51.2 |
| Leading | 00:41:20.4 | 00:41:47.7 |
| Trailing | 00:42:47.1 | 00:43:12.0 |
| Left-side background | 00:39:03.8 | 00:41:20.4 |
| Right-side background | 00:43:12.0 | 00:45:34.8 |

quantities in the intervals before the leading and after the trailing regions.

In order to quantify the influence of the switchback on the kinetic physics, we show in panel (d) of Figure 4 the deviation of the ion VDFs from the thermodynamic equilibrium by means of the parameter ϵ , namely, the non-Maxwellianity, for both protons (green) and alpha particles (violet), defined as (Greco et al. 2012; Valentini et al. 2016)

$$\epsilon_s = \frac{1}{n_s} \sqrt{\int (f_s - g_s)^2 d^3v}, \quad (2)$$

where n_s is the density for a species s , f_s is the measured VDF, and g_s is the associated Maxwellian distribution with the same density, temperature, and velocity as the observed one. In order to have a dimensionless quantity, the values of ϵ , for both protons and alpha particles, have been multiplied by $V_A^{3/2}$, V_A being the background Alfvén speed (Valentini et al. 2016) calculated by using the total ion mass density (Marsch et al. 1982). It is worth pointing out that in order to reduce the noise associated with the low count statistics, which can artificially increase the non-Maxwellianity (Graham et al. 2021), we removed the bins with less than three counts (one count) when proton (alpha particle) VDFs are considered. We find an increase of the non-Maxwellianity inside the switchback for the proton population, while alpha particles seem not to be strongly affected, in terms of deformation of the VDF, by the presence of the structure. For both species, we observe a more fluctuating behavior in the left background region. Moreover, we find that the values of ϵ are higher for alpha particles with respect to protons. This is a signature already observed in numerical experiments, which suggest that the alpha particle vortical motion may play a significant role in, or may be significantly affected by, a differential heating process (Valentini et al. 2016). These features can be explained in terms of magnetic reconnection events (Matthaeus 1982), where both magnetic and velocity shears can trigger non-Maxwellian and thermal processes.

Finally, in panel (e), we show another parameter, M , which is dimensionless and gives another indication on the non-Maxwellianity of the ion VDFs. M is defined as (Kaufmann & Paterson 2009; Pezzi et al. 2021)

$$M_s = \frac{2}{3n_s} \frac{\mathcal{S}_{g_s} - \mathcal{S}_{f_s}}{k_B}, \quad (3)$$

where k_B is Boltzmann's constant and \mathcal{S} is the kinetic entropy density, defined as

$$\mathcal{S}_{f_s} = -k_B \int d^3v f_s \log f_s. \quad (4)$$

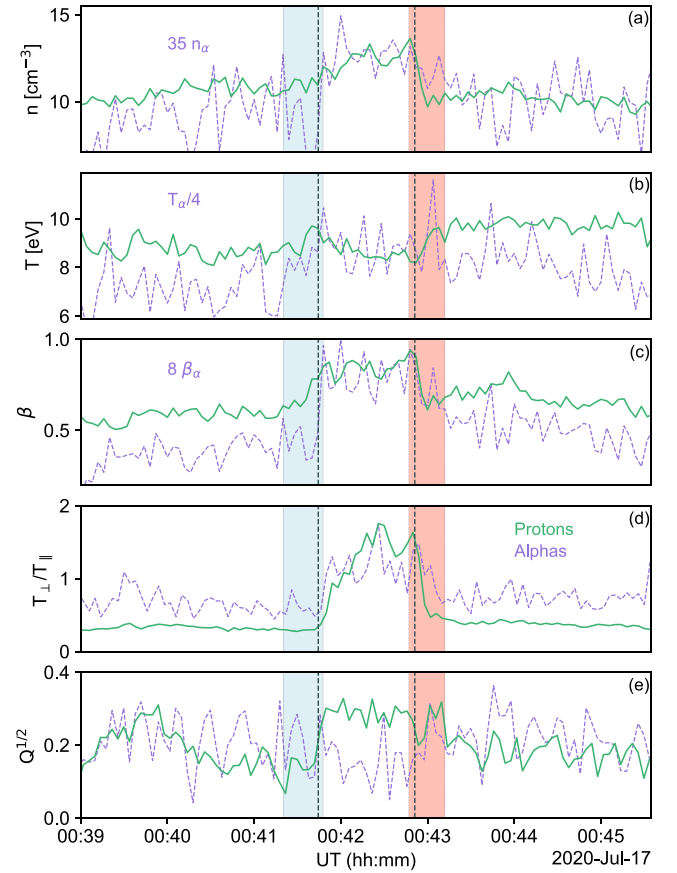


Figure 5. Ion density (a), temperature (b), plasma beta (c), temperature anisotropy (d), and agyrotropy (e) for both protons (green) and alpha particles (violet) around the isolated switchback of Figure 4. Blue and red shaded bands denote the leading and trailing regions, respectively, while vertical dashed lines delimit the structure, as in Figure 4.

Since the Maxwellian distribution has the maximum entropy, M is positive definite. We observe a deviation from the Maxwellianity for both protons and alpha particles inside the switchback, unlike what we found for ϵ . It is worth pointing out that, although both M and ϵ give information on the non-Maxwellian shape of the ion VDFs, M also includes the contribution of the heating. Then, in panel (e), we observe that M_p fluctuates inside the structure, while M_α has an abrupt increase (decrease) at the leading (trailing) edge of the switchback and is almost constant inside it.

In order to understand how the surrounding plasma reacts to the presence of this isolated switchback, in Figure 5, we show ion parameters for both protons (green) and alpha particles (violet). In the first three panels, alpha particle parameters have been rescaled for a better comparison with the proton parameters. Panel (a) shows the behavior of the ion density, which increases for both protons and alpha particles at the structure, suggesting the presence of wave activity (Stix 1992). Indeed, the correlation between density and magnetic field variations can be used in wave mode identification (fast magnetosonic waves or slow modes), as has been done by Chaston et al. (2020) on Parker Solar Probe measurements during the first encounter. By using wave decomposition in MHD approximation, they found that the major wave mode belongs to shear Alfvén waves. A different behavior between species is recovered for the temperature in panel (b). Indeed,

for alpha particles, we observe an increase related to the switchback, while for protons, the temperature remains almost stable. This feature, linked to the results for ϵ (panel (d) of Figure 4), suggests that the presence of a switchback could produce heating for the alphas, while for protons, it could play a role in the deformation of the VDF. We will discuss this point further later in the paper.

Moreover, panel (c) shows that the ion plasma beta is higher inside the switchback than outside, in agreement with the statistical analysis presented by Larosa et al. (2021), who suggested that higher values of β may be caused by a temperature anisotropy rather than by a higher temperature inside the switchbacks. This is indeed the case, since we observe an abrupt change in the temperature anisotropy, T_{\perp}/T_{\parallel} , inside the structure (panel (d)) for both protons and alpha particles. In particular, outside the structure, $T_{\perp}/T_{\parallel} < 1$, while inside, $T_{\perp}/T_{\parallel} > 1$, even if for alphas $T_{\perp}/T_{\parallel} \gtrsim 1$. It is worth pointing out that parallel and perpendicular directions are evaluated with respect to the background magnetic field to avoid the effects of the variation of the magnetic field during the switchback. Focusing for now only on protons, by using the background field to evaluate the direction of temperature anisotropy, we find that outside the structure, $T_{\perp}/T_{\parallel} \simeq 0.3$, while inside, T_{\perp}/T_{\parallel} reaches values of 1.7. On the other hand, if we consider the local magnetic field, the temperature anisotropy moves from 0.3 outside the structure to 0.5 inside the structure. This is expected since the presence of the secondary beam forces the temperature anisotropy to be in the parallel direction, since the beam follows the direction of the magnetic field and the VDF is elongated in the direction parallel to the magnetic field. However, if we consider the temperature anisotropy of only the proton core with respect to the local magnetic field, we find that T_{\perp}/T_{\parallel} moves from 1 outside the structure to about 1.3 (with peaks of 1.5) inside the structure.

Finally, in panel (e), we show the ion agyrotropy, $Q^{1/2}$, defined as (Swisdak 2016)

$$Q = \frac{P_{xy}^2 + P_{xz}^2 + P_{yz}^2}{P_{\perp}^2 + 2P_{\parallel}P_{\parallel}}, \quad (5)$$

where P_{ij} are the components of the ion (protons and alpha particles) pressure tensor in the reference frame in which one of the axes is along the direction of the background magnetic field and the two perpendicular pressures are the same. For a gyrotropic distribution function, $Q = 0$, while for the maximal departure from gyrotropy, $Q = 1$. As in the case of ϵ , we observe an enhancement of the agyrotropy, $Q^{1/2}$, at the switchback for the proton population, while alpha particles have an almost constant value of $Q^{1/2}$ in the considered interval of Figure 5. However, it is worth noting that, for alpha particles, we observe a reduction of $Q^{1/2}$ within the structure, even if the general behavior of the agyrotropy is characterized by strong fluctuations. The emerging picture suggests that within the switchback, alphas are heated, and their VDF tends to recover a more regular shape, toward isotropy.

3.1. Proton and Alpha Particle VDFs

The parameters associated with the deformation of the ion VDFs, namely, ϵ (panel (d) of Figure 4) and $Q^{1/2}$ (panel (e) of Figure 5), have suggested that protons and alpha particles react differently to the presence of switchbacks. To better investigate

the distortion of the 3D ion VDFs, in Figures 6 and 7, we show an example of 2D contour plots (integrated along the out-of-plane direction) of proton and alpha particle VDFs, respectively, at the two points marked by red stars in Figure 4, namely, in the left background region (top panels) and inside the switchback (bottom panels). The reduced ion VDFs are represented in the reference frame of the background magnetic field, while the black arrow in each panel denotes the local direction of the magnetic field in this reference frame. Moreover, VDFs of each ion population are plotted in their respective rest frame. We also point out the different scales of the color bars for each of the two species, which recall the fact that alpha particles are only $\sim 3\%$ of the proton population.

Outside the structure, at about 00:41, both ϵ_p and ϵ_{α} (see panel (d) of Figure 4) do not significantly deviate from the thermodynamic equilibrium. However, we find $\epsilon_{\alpha} > \epsilon_p$, which results in a more distorted shape for the alpha particle VDF with respect to the proton one. Indeed, for protons, we observe a clear and stable field-aligned beam, panels (a) and (b) of Figure 6. The direction of the secondary beam is along both the background and local magnetic field, where the latter is evaluated as an average over 1 s around the time of the considered VDF (which corresponds approximately to the time of acquisition of the 3D VDF by PAS). In the plane perpendicular to the background magnetic field, the proton VDF is almost gyrotropic, as already suggested by $Q^{1/2}$. On the other hand, although the alpha particle VDF shows the presence of a secondary field-aligned beam as well (see panels (a) and (b) of Figure 7), in general the VDF is more distorted both in the plane that contains the magnetic field vector and in the plane perpendicular to it, namely, $\epsilon_{\alpha} > \epsilon_p$ and $Q_{\alpha}^{1/2} > Q_p^{1/2}$, respectively.

Inside the structure, at about 00:42, the behavior described above changes. In particular, we find that protons are significantly affected by the presence of the switchback, while alpha particles are less affected. Indeed, both parameters related to the VDF distortion are larger for protons, namely, $\epsilon_p > \epsilon_{\alpha}$ and $Q_p^{1/2} > Q_{\alpha}^{1/2}$. The proton VDF shows a change in the direction of the temperature anisotropy from $T_{\perp}/T_{\parallel} < 1$, due to the presence of a well-defined secondary beam, in the region outside the switchback, to $T_{\perp}/T_{\parallel} > 1$ inside the structure. For the latter, we find an elongated VDF in the direction perpendicular to the background magnetic field (see panels (d) and (e) of Figure 6), with no clear presence of the secondary beam. Moreover, also in the plane perpendicular to the background magnetic field (panel (f) of Figure 6), the proton VDF is not gyrotropic, and it shows an elongation in the direction parallel to the local magnetic field (see black arrow). Although alpha particles show features as similar as protons for the agyrotropy (see panels (d) and (e) of Figure 7), a different behavior is observed in the planes that contain the background magnetic field, since no clear signatures in the temperature anisotropy are found, being $T_{\perp}/T_{\parallel} \simeq 1$, with no preferential directions, even if the VDF looks deformed with respect to a Maxwellian (notice that the latter aspect can also be influenced by low counts).

To better interpret the distortion of ion VDFs, we now consider separately the core and the beam of both protons and alpha particles (Bruno et al. 2024). In particular, panel (a) of Figure 8 shows the relative number density of the secondary beam, n_b , with respect to the core, n_c , for both protons (green) and alpha particles (violet). We observe for both ion

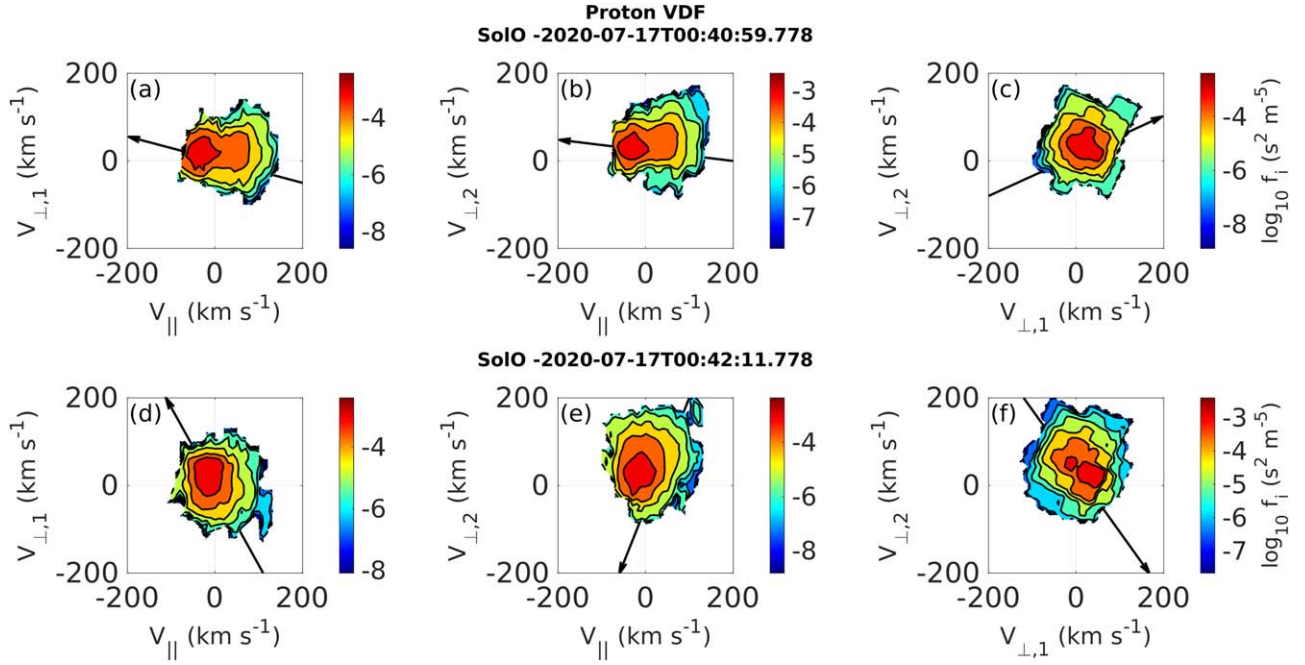


Figure 6. Two-dimensional contour plots of the reduced proton VDFs in the reference frame of the background magnetic field in the two points marked by red stars in Figure 4, namely, in the left background region (top panels) and inside the switchback (bottom panels). In each panel, the black arrow denotes the local direction of the magnetic field in the reference frame used to show the VDFs.

populations an increase of the relative beam density inside the structure. This is in disagreement with the results presented by Louarn et al. (2021), since they found a decrease of the proton beam relative density by a factor of ~ 4 . They modeled the proton distribution, after removing alpha particles, by a bi-Maxwellian core and an asymmetric beam in the parallel direction. Moreover, the alpha population is typically detected for energy above 1500 eV, and it is removed from the total ion VDF just considering this energy as a threshold between the two populations. However, an alpha particle low-energy extension is occasionally seen in the spectrogram (Louarn et al. 2021). In our case, we separate proton and alpha particle populations by using a machine learning technique, which is also able to separate the core and beam for both ion species, without using any fitting procedure or energy constraints for the separation of the two ion populations. In particular, we use the statistical technique of clustering, which is one of the most widely used forms of unsupervised machine learning for grouping data based on a predefined set of characteristics, since it is able to reveal underlying patterns in the data. Indeed, clustering tries to identify subpopulations within the overall data set, assigning to each observation a probability of belonging to a certain group. Then, the portion of the total VDF belonging to each ion family can be determined, even in the presence of overlap. All the details about the machine learning technique and the validation for the data used in the present paper can be found in De Marco et al. (2023) and Bruno et al. (2024).

Finally, the relative drift speed between the ion beam and core, normalized to the background Alfvén speed, shown in panel (b) of Figure 8, has an opposite behavior with respect to the relative number density of the secondary beam, with $|V_b - V_c|/V_A$ that decreases inside the switchback. It worth pointing out that alpha particle data are noisier with respect to the proton ones, first of all for their lower counts, as already discussed, but also because sometimes the presence of a

secondary beam for alpha particles is not very clear, unlike in the case of protons. Thus, Figure 8 suggests that switchbacks play a role in ion heating, i.e., an increase of the temperature evaluated as the moment of the total (core plus beam) VDF, in particular for alpha particles (see panel (b) of Figure 5), with the appearance of a denser secondary beam and a smaller relative drift speed between the beam and core. The mechanism at work is still under investigation, but it seems that in the leading and trailing edges, where the discontinuities appear, some local processes could produce an exchange of particles and a corresponding speed reduction between the core and beam, more important for alpha particles than for protons. In the future, we will study magnetic and electric fluctuations at small scales in the leading and trailing edges of switchbacks but not for this specific isolated magnetic deflection, since the data from the Radio and Plasma Waves instrument are not available.

4. Summary and Discussions

The Parker Solar Probe mission has revealed the ubiquitous presence of a large number of S-shaped magnetic structures that produce patches of large, intermittent magnetic field reversals, namely, switchbacks, in the inner heliosphere. Now, thanks also to Solar Orbiter, the kinetic properties of ions related to the presence of switchbacks can be investigated in detail, taking into account the ion VDFs from the PAS of the SWA suite. It is worth pointing out that, for the investigation of the ion kinetic effects, it is crucial to be able to correctly separate the different ion species. The general approach is to use a fitting procedure on the ion VDFs. Using Parker Solar Probe measurements, scientists mainly focused on the proton core, fitting a model bi-Maxwellian to 3D proton VDFs measured by SPAN-Ai, and complementing these fits with data from the Solar Probe Cup instrument (see, e.g., Woodham et al. 2021; Laker et al. 2024). Recently, they started including the contribution of heavy ions by fitting protons (core and beam)

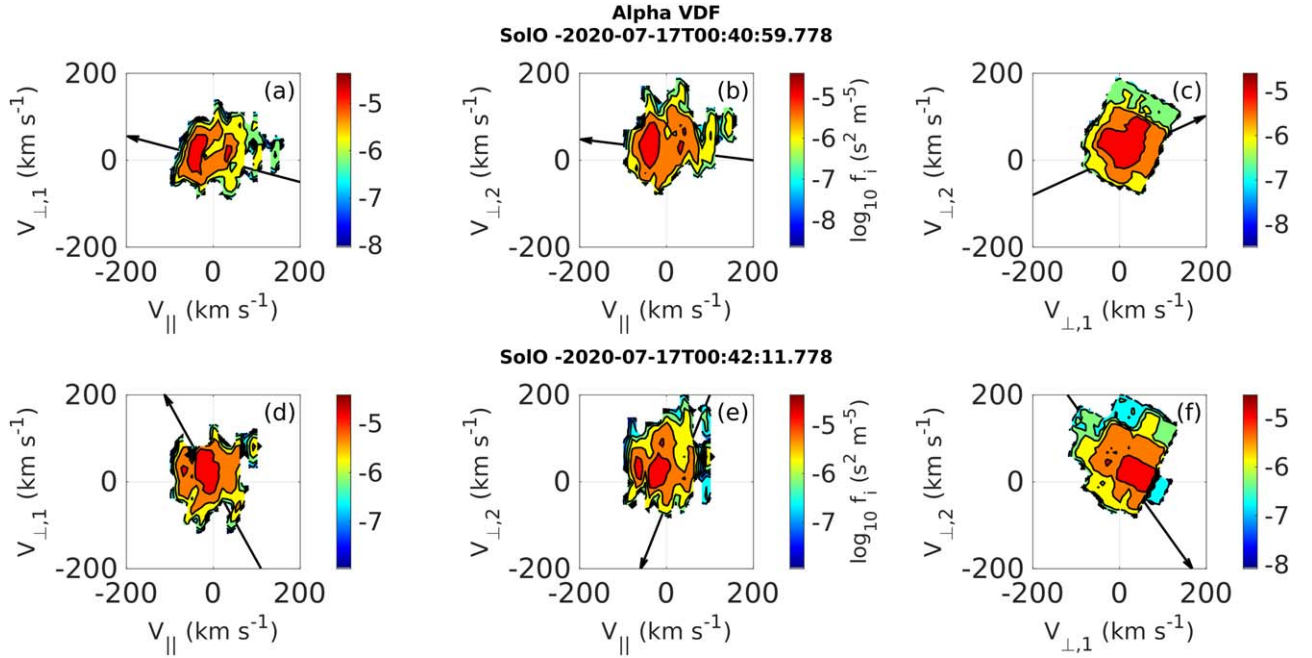


Figure 7. Two-dimensional contour plots of the reduced alpha particle VDFs in the reference frame of the background magnetic field in the two points marked by red stars in Figure 4, namely, in the left background region (top panels) and inside the switchback (bottom panels). In each panel, the black arrow denotes the local direction of the magnetic field in the reference frame used to show the VDFs.

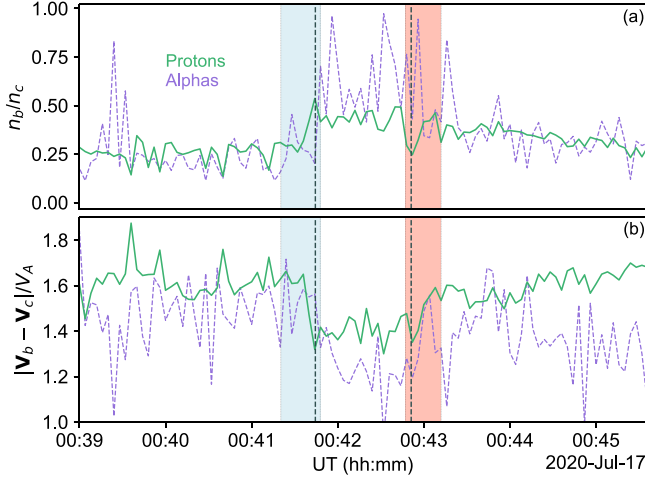


Figure 8. Density ratio (a) and drift speed normalized to the background Alfvén speed (b) between the secondary beam and the core for both protons (green) and alpha particles (violet).

and alpha particles (McManus et al. 2022; Huang et al. 2023a). Very recently, McManus et al. (2024) also applied a bi-Maxwellian fitting model for the alpha core and beam. Using Solar Orbiter measurements, scientists modeled the proton distributions measured by PAS by a bi-Maxwellian core and an asymmetric beam in the parallel direction, after removing alpha particles considering a particular value of energy as a threshold between the two populations (Louarn et al. 2021). Fitting procedures rely on approximating the distribution function with an ideal bi-Maxwellian, which would de facto constrain the physics embedded in the solar wind. Moreover, other constraints are set in order to find a stable solution. Furthermore, most of the time the particle energy spectra of the protons and the alpha particles overlap, producing uncertainty in the identification of the different populations.

There are cases when the overlap is so strong that the fitting procedure cannot be applied and only estimates can be obtained, at least for protons and alphas, usually by splitting the VDF at specific values of energy. Here, we use an alternative approach based on the statistical technique of clustering, a standard tool in many data-driven and machine learning applications, which has been applied to the full 3D VDFs measured by PAS to separate the core and beam for both protons and alpha particles (De Marco et al. 2023; Bruno et al. 2024). It is worth pointing out that the results of the clustering are not without ambiguities, and human oversight is still needed in the final stage for science-level data. However, the machine learning technique used to separate the different ion populations is a powerful tool that can complement and strengthen traditional fittings.

In this paper, we investigate the ion kinetic properties as a reaction to the presence of switchbacks, focusing on a case study, picking up an isolated, large-scale magnetic deflection on 2020 July 17, when Solar Orbiter was embedded in the rarefaction region of a slow Alfvénic stream at 0.64 au. This strong structure is characterized by high values of z , with a maximum value of 0.67, corresponding to a magnetic deflection of about 150° , close to an almost full reversal. Moreover, the selected isolated switchback lasts, considering the leading and trailing edges, less than 2 minutes. Apart from the expected correlation between the magnetic deflection and the spike in the ion speed, due to the Alfvénic nature of the switchbacks, we found a certain correlation between the switchback and both proton and alpha particle densities, which suggests wave activity. However, the most interesting correlation we found is between the magnetic deflection and alpha particle temperature (no correlation with proton temperature), suggesting a role of switchbacks in preferentially heating heavy ions.

Our results are in disagreement with existing studies that use Parker Solar Probe observations (see, e.g., Woodham et al.

2021; Huang et al. 2023a; Laker et al. 2024) mainly related to the behavior of the ion temperature as discussed in the Introduction (Section 1). In our opinion, these differences can be due to different reasons, such as (i) the intensity and duration of the considered magnetic field deflections, (ii) the heliospheric radial distance at which switchbacks are observed, and, more importantly, (iii) the ion measurements used for the analysis. The latter has already been discussed above in detail. For the other points, we would like to highlight that, in previous studies, the authors mainly consider patches of switchbacks that last for tens of minutes, such as in Woodham et al. (2021), where the majority of the switchback structures do not rotate more than 90° , or in Huang et al. (2023a), where fully reversed structures are considered, but the deflection is only in the radial magnetic component. On the other hand, Woolley et al. (2020) identified individual switchbacks with a full 180° rotation in \mathbf{B} showing that the parallel temperature inside the structures does not change with respect to the outside value. The dependence of the change in temperature on the magnetic field angle has been studied by Laker et al. (2024), suggesting that the temperature enhancement can be created by some in situ mechanisms at work in the near-Sun environment. Another important difference between our analysis and previous studies based on Parker Solar Probe observations is the heliospheric radial distance. Indeed, all previous Parker Solar Probe studies on switchbacks refer to a near-Sun solar wind (<0.2 au), while, in our case, Solar Orbiter was embedded in a slow Alfvénic wind at 0.64 au. Finally, although it is reasonable that the kinetic features related to switchbacks could depend on the solar wind conditions, since the latter are strongly related to source regions on the Sun, in this case, they cannot explain the observed differences between our results and previous studies. Indeed, the cited studies on switchbacks focused on slow Alfvénic wind, since, most of the time, Parker Solar Probe was embedded in this kind of wind.




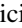

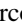
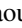


In addition to the standard quantities to look at the shape of the ion VDFs, namely, temperature anisotropy and agyrotropy, we employ some parameters to measure higher-order VDF disturbances from the local Maxwellian beyond its second-order moment. These parameters retain information about dissipation, since high-order variations from the Maxwellian coincide with the presence of fine velocity-space structures that, in turn, are dissipated by collisional effects (Pezzi et al. 2016). We found that the switchback is associated with strong deformations of the ion VDFs, in particular for protons inside the structure, with the presence of a well-defined beam. Our results on the kinetic properties of ions related to the case study suggest that the deformation of the ion VDFs is the effect of processes that affect both core and beam. Therefore, it is crucial to have information separately for core and beam for both protons and alpha particles. Thanks to the statistical technique of clustering (De Marco et al. 2023; Bruno et al. 2024), we found an increase of the relative beam density and a decrease of the relative drift speed between the core and beam inside the switchback. These results, associated with the increase of temperature observed for the alphas, suggest a preferential heating of heavy ions due to a denser secondary beam and a smaller separation between the beam and core. These results provide insight into the heating problem in collisionless plasmas, allowing us to add new pieces to the puzzle of the energy dissipation mechanisms in the solar wind. However, several questions are still open, and a statistical analysis

pointing to the relationship between switchbacks and kinetic effects is required and will be the subject of a future work.

Acknowledgments

D.P. acknowledges the support of the PRIN 2022 project “2022KL38BK—The ULtimate fate of TuRbulence from space to laboratory plAsmas (ULTRA)” (Master CUP B53D2300 4850006; CUP F53D23001220008) by the Italian Ministry of University and Research, “Finanziato dall’Unione europea—Next Generation EU” Piano Nazionale di Ripresa e Resilienza (PNRR) Missione 4 “Istruzione e Ricerca” - Componente C2 Investimento 1.1, “Fondo per il Programma Nazionale di Ricerca e Progetti di Rilevante Interesse Nazionale (PRIN)” Settore PE09. S.P. acknowledges the project “Data-based predictions of solar energetic particle arrival to the Earth: ensuring space data and technology integrity from hazardous solar activity events” (CUP H53D23011020001) “Finanziato dall’Unione europea—Next Generation EU” Piano Nazionale di Ripresa e Resilienza (PNRR) Missione 4 “Istruzione e Ricerca” - Componente C2 Investimento 1.1, “Fondo per il Programma Nazionale di Ricerca e Progetti di Rilevante Interesse Nazionale (PRIN)” Settore PE09. D.P., A.S., and R. D.A. would like to acknowledge the International Space Science Institute (ISSI) for its support of the team #550 “Solar sources and evolution of the Alfvénic slow wind” dedicated in part to the analysis of Solar Orbiter data.

ORCID iDs

Denise Perrone  <https://orcid.org/0000-0003-1059-4853>
 Adriana Settino  <https://orcid.org/0000-0003-1821-7390>
 Silvia Perri  <https://orcid.org/0000-0002-8399-3268>
 Raffaella D’Amicis  <https://orcid.org/0000-0003-2647-117X>
 Rossana De Marco  <https://orcid.org/0000-0002-7426-7379>
 Georgios Nicolaou  <https://orcid.org/0000-0003-3623-4928>
 Daniele Telloni  <https://orcid.org/0000-0002-6710-8142>
 Roberto Bruno  <https://orcid.org/0000-0002-2152-0115>
 Christopher J. Owen  <https://orcid.org/0000-0002-5982-4667>

References

- Agapitov, O. V., Drake, J. F., Swisdak, M., et al. 2022, *ApJ*, **925**, 213
 Akhavan-Tafti, M., Kasper, J., Huang, J., & Bale, S. D. 2021, *A&A*, **650**, A4
 Bale, S. D., Badman, S. T., Bonnell, J. W., et al. 2019, *Natur*, **576**, 237
 Balogh, A., Forsyth, R. J., Lucek, E. A., Horbury, T. S., & Smith, E. J. 1999, *GeoRL*, **26**, 631
 Bizien, N., Dudok de Wit, T., Froment, C., et al. 2023, *ApJ*, **958**, 23
 Borovsky, J. E. 2016, *JGRA*, **121**, 5055
 Bruno, R., Marco, R. D., D’Amicis, R., et al. 2024, *ApJ*, **969**, 106
 Chaston, C. C., Bonnell, J. W., Bale, S. D., et al. 2020, *ApJS*, **246**, 71
 D’Amicis, R., Bruno, R., Panasenco, O., et al. 2021, *A&A*, **656**, A21
 De Marco, R., Bruno, R., Jagarlamudi, V. K., et al. 2023, *A&A*, **669**, A108
 de Pablos, D., Samanta, T., Badman, S. T., et al. 2022, *SoPh*, **297**, 90
 Drake, J. F., Agapitov, O., Swisdak, M., et al. 2021, *A&A*, **650**, A2
 Dudok de Wit, T., Krasnoselskikh, V. V., Bale, S. D., et al. 2020, *ApJS*, **246**, 39
 Fargette, N., Lavraud, B., Rouillard, A. P., et al. 2022, *A&A*, **663**, A109
 Fargette, N., Lavraud, B., Øieroset, M., et al. 2020, *GeoRL*, **47**, e86726
 Farrell, W. M., Rasca, A. P., MacDowall, R. J., et al. 2021, *ApJ*, **915**, 68
 Fedorov, A., Louarn, P., Owen, C. J., et al. 2021, *A&A*, **656**, A40
 Fisk, L. A., & Kasper, J. C. 2020, *ApJL*, **894**, L4
 Fox, N. J., Velli, M. C., Bale, S. D., et al. 2016, *SSRv*, **204**, 7
 Froment, C., Krasnoselskikh, V., Dudok de Wit, T., et al. 2021, *A&A*, **650**, A5
 Graham, D. B., Khotyaintsev, Y. V., André, M., et al. 2021, *JGRA*, **126**, e29260

- Greco, A., Valentini, F., Servidio, S., & Matthaeus, W. H. 2012, [PhRvE](#), **86**, 066405
- Horbury, T. S., Matteini, L., & Stansby, D. 2018, [MNRAS](#), **478**, 1980
- Horbury, T. S., Woolley, T., Laker, R., et al. 2020a, [ApJS](#), **246**, 45
- Horbury, T. S., O'Brien, H., Carrasco Blazquez, I., et al. 2020b, [A&A](#), **642**, A9
- Huang, J., Kasper, J. C., Larson, D. E., et al. 2023a, [ApJ](#), **954**, 133
- Huang, J., Kasper, J. C., Fisk, L. A., et al. 2023b, [ApJ](#), **952**, 33
- Kasper, J. C., Bale, S. D., Belcher, J. W., et al. 2019, [Natur](#), **576**, 228
- Kasper, J. C., Klein, K. G., Lichko, E., et al. 2021, [PhRvL](#), **127**, 255101
- Kaufmann, R. L., & Paterson, W. R. 2009, [JGRA](#), **114**, A00D04
- Krasnoselskikh, V., Larosa, A., Agapitov, O., et al. 2020, [ApJ](#), **893**, 93
- Laker, R., Horbury, T. S., Woodham, L. D., Bale, S. D., & Matteini, L. 2024, [MNRAS](#), **527**, 10440
- Laker, R., Horbury, T. S., Bale, S. D., et al. 2021, [A&A](#), **650**, A1
- Larosa, A., Krasnoselskikh, V., Dudok de Wit, T., et al. 2021, [A&A](#), **650**, A3
- Louarn, P., Fedorov, A., Prech, L., et al. 2021, [A&A](#), **656**, A36
- Macneil, A. R., Owens, M. J., Wicks, R. T., & Lockwood, M. 2021, [MNRAS](#), **501**, 5379
- Mallet, A., Squire, J., Chandran, B. D. G., Bowen, T., & Bale, S. D. 2021, [ApJ](#), **918**, 62
- Marsch, E., Muhlhauser, K.-., Rosenbauer, H., Schwenn, R., & Neubauer, F. M. 1982, [JGR](#), **87**, 35
- Martinović, M. M., Klein, K. G., Huang, J., et al. 2021, [ApJ](#), **912**, 28
- Matthaeus, W. H. 1982, [GeoRL](#), **9**, 660
- McManus, M. D., Bowen, T. A., Mallet, A., et al. 2020, [ApJS](#), **246**, 67
- McManus, M. D., Verniero, J., Bale, S. D., et al. 2022, [ApJ](#), **933**, 43
- McManus, M. D., Klein, K. G., Bale, S. D., et al. 2024, [ApJ](#), **961**, 142
- Mozer, F. S., Agapitov, O. V., Bale, S. D., et al. 2020, [ApJS](#), **246**, 68
- Müller, D., St., Cyr, O. C., Zouganelis, I., et al. 2020, [A&A](#), **642**, A1
- Nicolaou, G., Wicks, R. T., Owen, C. J., et al. 2021, [A&A](#), **656**, A10
- Nistico, G., Bothmer, V., Patsourakos, S., & Zimbardo, G. 2010, [AnGeo](#), **28**, 687
- Owen, C. J., Bruno, R., Livi, S., et al. 2020, [A&A](#), **642**, A16
- Panasenco, O., Velli, M., & Panasenco, A. 2019, [ApJ](#), **873**, 25
- Pecora, F., Matthaeus, W. H., Primavera, L., et al. 2022, [ApJL](#), **929**, L10
- Perrone, D., Settino, A., De Marco, R., D'Amicis, R., & Perri, S. 2023, [FrASS](#), **10**, 1250219
- Pezzi, O., Valentini, F., & Veltri, P. 2016, [PhRvL](#), **116**, 145001
- Pezzi, O., Liang, H., Juno, J. L., et al. 2021, [MNRAS](#), **505**, 4857
- Raouafi, N. E., Matteini, L., Squire, J., et al. 2023, [SSRv](#), **219**, 8
- Schwadron, N. A., & McComas, D. J. 2021, [ApJ](#), **909**, 95
- Squire, J., Chandran, B. D. G., & Meyrand, R. 2020, [ApJL](#), **891**, L2
- Stix, T. H. 1992, *Waves in plasmas* (New York: American Institute of Physics)
- Swisdak, M. 2016, [GeoRL](#), **43**, 43
- Telloni, D., Zank, G. P., Stangalini, M., et al. 2022, [ApJL](#), **936**, L25
- Valentini, F., Perrone, D., Stabile, S., et al. 2016, [NJPh](#), **18**, 125001
- Woodham, L. D., Horbury, T. S., Matteini, L., et al. 2021, [A&A](#), **650**, L1
- Woolley, T., Matteini, L., Horbury, T. S., et al. 2020, [MNRAS](#), **498**, 5524
- Wyper, P. F., DeVore, C. R., Antiochos, S. K., et al. 2022, [ApJL](#), **941**, L29
- Yamauchi, Y., Suess, S. T., Steinberg, J. T., & Sakurai, T. 2004, [JGRA](#), **109**, A03104
- Zank, G. P., Nakanotani, M., Zhao, L. L., Adhikari, L., & Kasper, J. 2020, [ApJ](#), **903**, 1